

Confinement-Induced Isosymmetric Metal-Insulator Transition in Ultrathin Epitaxial V_2O_3 Films

Simon Mellaerts¹, Claudio Bellani², Wei-Fan Hsu¹, Alberto Binetti¹, Koen Schouteden¹, Maria Recaman-Payo¹, Mariela Menghini^{1,3}, Juan Rubio Zuazo^{4,5}, Jesús López Sánchez^{4,5,6}, Jin Won Seo², Michel Houssa^{1,7} and Jean-Pierre Locquet¹

¹*Department of Physics and Astronomy, KU Leuven, Celestijnenlaan 200D,*

3001 Leuven, Belgium, ²*Department of Materials Engineering,*

KU Leuven, Kasteelpark Arenberg 44, 3001 Leuven,

Belgium, ³*IMDEA Nanociencia, Calle Faraday 9,*

E29049 Madrid, Spain, ⁴*BM25-SpLine, ESRF, France,*

⁵*Instituto de Ciencia de Materiales de Madrid (ICMM-CSIC),*

28049 Madrid, Spain, ⁶*Departamento de Electrocerámica,*

Instituto de Cerámica y Vidrio - Consejo Superior de Investigaciones Científicas (ICV-CSIC),
Calle Kelsen 5, 28049 Madrid, Spain, ⁷*Imec, Kapeldreef 75, 3001 Leuven, Belgium.**

Dimensional confinement has shown to be an effective strategy to tune competing degrees of freedom in complex oxides. Here, we achieved atomic layered growth of trigonal vanadium sesquioxide (V_2O_3) by means of oxygen-assisted molecular beam epitaxy. This led to a series of high-quality epitaxial ultrathin V_2O_3 films down to unit cell thickness, enabling the study of the intrinsic electron correlations upon confinement. By electrical and optical measurements, we demonstrate a dimensional confinement-induced metal-insulator transition in these ultrathin films. We shed light on the Mott-Hubbard nature of this transition, revealing an abrupt vanishing of the quasiparticle weight as demonstrated by photoemission spectroscopy. Furthermore, we prove that dimensional confinement acts as an effective out-of-plane stress. This highlights the structural component of correlated oxides in a confined architecture, while opening an avenue to control both in-plane and out-of-plane lattice components by epitaxial strain and confinement, respectively.

I. INTRODUCTION

The richness of transition metal oxides emerges from the strong interplay of many degrees of freedom leading to competing ground states, whose energy landscape can be deformed by temperature, pressure, and many other external parameters. The room-temperature (RT) metal-insulator transition (MIT) in vanadium sesquioxide (V_2O_3) is a key example of an isosymmetric Mott transition which can be induced by pressure, temperature, epitaxial strain and Cr doping [1–5]. For the latter approach, extended X-ray absorption fine-structure spectroscopy (EXAFS) has shown that this RT MIT involves a local trigonal distortion that results in a long-range strain driving an abrupt change in the c/a ratio [2, 6].

On an electronic level, the octahedral crystal field (CF) of V $3d$ with a lower triple-degenerate t_{2g} and upper two-fold degenerate e_g^σ orbital levels undergoes a symmetry lowering of the former t_{2g} level into an a_{1g} singlet pointing along the c axis and a lower e_g^π doublet in the basal plane due to the trigonal distortion. This distortion leads to an enhanced CF splitting between a_{1g} and e_g^π driving the electronic MIT, as also shown by dynamical mean-field theory (DMFT) calculations [7].

With the advances in high-quality and layer-by-layer epitaxial growth of ultrathin films and heterostructures, a vast playground has become available to tune these orbital degrees of freedom, which are extremely sensitive

to hybridization, CF and the local atomic environment [8, 9]. Ultimately, this opens the possibility towards the stabilization of a single atomic layer of V_2O_3 with the promise of a high-temperature ferromagnetic Chern insulator [10].

In this work, we propose dimensional confinement as an alternative pressure term to tune the RT MIT in V_2O_3 . High-quality ultrathin V_2O_3 films were grown coherently on Al_2O_3 (0001) substrates with thickness ranging from 6 – 18 monolayers (MLs) (1.4 – 4.2 nm) by the use of oxygen-assisted molecular beam epitaxy (MBE). It is shown that the out-of-plane confinement in these ultrathin films induces an intrinsic isosymmetric MIT at RT. By the use of photoemission spectroscopy (PES), we prove the bandwidth-controlled nature of this transition with an abrupt vanishing of the quasiparticle (QP) weight at the Fermi level. Subsequently, Raman spectroscopy and synchrotron X-ray diffraction show the stress-induced nature of this transition.

II. METHODS

All thin films were deposited on (0001)- Al_2O_3 by means of oxygen-assisted MBE in ultrahigh vacuum (UHV) conditions with the growth chamber at base pressure of 10^{-10} mbar. MBE growth was monitored in-situ by the use of reflection high-energy electron diffraction (RHEED).

Chemical characterization was performed (without ex-

* simon.mellaerts@kuleuven.be

posure to ambient air) by X-ray photoelectron spectroscopy (XPS) in an UHV FlexMod SPECS system equipped with a monochromatic 100 W Al source ($E = 1486.7$ eV), operating at a base pressure 10^{-10} mbar. The XPS spectra were recorded with stepsize 0.05 eV and pass energy 20 eV. The morphology of the ultrathin films was characterized by atomic force microscopy (AFM) (ParkXE-100 AFM) under ambient conditions at RT. AFM images were recorded in non-contact mode with the use of Si probes. The structural properties of the samples were characterized by means of X-ray reflection (XRR) and reciprocal space mapping (RSM) with a Panalytical X'pert Pro diffractometer using a Cu anode with $K_{\alpha 1}$ radiation.

Temperature-dependent resistivity measurements in the Van der Pauw configuration were performed in an Oxford Optistat CF2-V cryostat with a Keithley 4200-SCS parameter analyzer. Simultaneous Fourier-transform infrared (FTIR) spectroscopy measurements with a Bruker Vertex V80 were taken as a function of temperature, controlled by a thermocoupler. Angle-resolved ultraviolet photoelectron spectroscopy (ARUPS) was performed in the UHV FlexMod SPECS system at RT using a UVS300 high-intensity vacuum ultraviolet light source optimized for He-II radiation ($E = 40.8$ eV). The ARUPS spectra were recorded with stepsize of 0.01 eV and pass energy of 30 eV. Raman spectra were acquired by a confocal Raman microscope Witec ALPHA model 300RA (Oxford instruments, Abingdon, UK) with a Nd:YAG green laser source of 532 nm in p-polarization. Samples were placed on a piezo-driven scan platform with a high positioning accuracy of 4 nm and 0.5 nm in lateral and vertical directions, respectively. Raman scans were carried out at RT using a $100\times$ objective with a numerical aperture of 0.95. The output laser power was 40 mW to minimize overheating effects and sample damage. Spectra were collected in the spectral range $65\text{-}3850$ cm^{-1} by using a 600 g mm^{-1} grating. Subsequently, raw data were processed by the Witec Project Plus software (version 2.08).

Synchrotron radiation high-resolution X-Ray diffraction were performed at the SpLine CRG BM25 beamline at the ESRF The European Synchrotron (Grenoble, France). The wavelength of the X-ray beam was 0.496 Å. Measurements were carried out in reflection geometry using a six-circle diffractometer in vertical configuration. XRD patterns were collected between the range of 5° - 45° (2θ) using a 2D photon-counting X-ray MAXIPIX detector [11].

III. RESULTS

A. High-quality growth of epitaxial ultrathin films

To study novel electronic phenomena in strongly correlated electron systems where many energy scales com-

pete in defining the ground state, there is the need for the growth of high-quality films up to atomic layer precision. In this respect, MBE has shown to be one of the most successful compared to other deposition techniques. By in-situ monitoring the RHEED pattern during the growth, we confirm the epitaxial growth of the ultrathin films on atomically flat (0001)- Al_2O_3 substrates. In addition, intensity oscillations in the RHEED are observed (see Figure 1b) with a periodicity corresponding to the expected growth of one atomic layer, calibrated by the e-beam flux and oxygen pressure. Hence, this corundum V_2O_3 material with conventional unit cell (UC) consisting of 6 ML (see Figure 1a) can be grown in a ML fashion, with the ability to control the thickness down to atomic layer precision. This ML growth is also evident from AFM images shown in Figure 1c with estimated step terraces of width 32 nm.

The lattice mismatch of the epitaxial V_2O_3 films with the Al_2O_3 substrates leads to an in-plane compressive strain of 4.2%. By RSM in $(10\bar{1}10)$ reflection, it is shown that the ultrathin films are fully strained in a coherent manner without any strain relaxation. This is due to the fact that all films are below the critical thickness. Hence, in the comparison between the different ultrathin films an identical in-plane lattice constant can be assumed.

Vanadium oxides are known to have a rich phase diagram with many different oxidation states to be stabilized [12, 13]. Therefore, XPS was performed immediately after growth without exposure to ambient air to prevent further oxidation of the films. The core level O $1s$ - V $2p$ spectrum is shown in Figure 1e with corresponding curve fitting, confirming the V^{3+} stoichiometry (see Fig. S1 of the Supplemental Material for detailed analysis). Alternatively the binding energy difference between O $1s$ and V $2p_{3/2}$ equals 14.5 eV, which also confirms this stoichiometry [14]. Also note that the broadened linewidth of the V $2p_{3/2}$ core state can be ascribed to the presence of the electron correlations in the $3d$, rather than a mixed oxidation state [15]. Moreover, a comparison of core level XPS spectra of the different ultrathin films proves that stoichiometry has been preserved for all thicknesses (see Figure 1f). This excludes any changes as a function of the thickness to be ascribed to a change in the oxygen stoichiometry of the films. Nonetheless, a reducing linewidth of the V $2p_{3/2}$ core level is observed upon thickness reduction (see inset of Fig. 1f), suggesting the diminishment of the electron correlations, which is indeed the case as will be shown in the subsequent sections.

In contrast to earlier reports on ultrathin V_2O_3 films [16, 17], we prove an atomic layer control in the growth of epitaxial coherent and stoichiometric V_2O_3 in the ultrathin limit. Hence, this permits the study of the intrinsic properties of this archetypical Mott material in the few MLs limit.

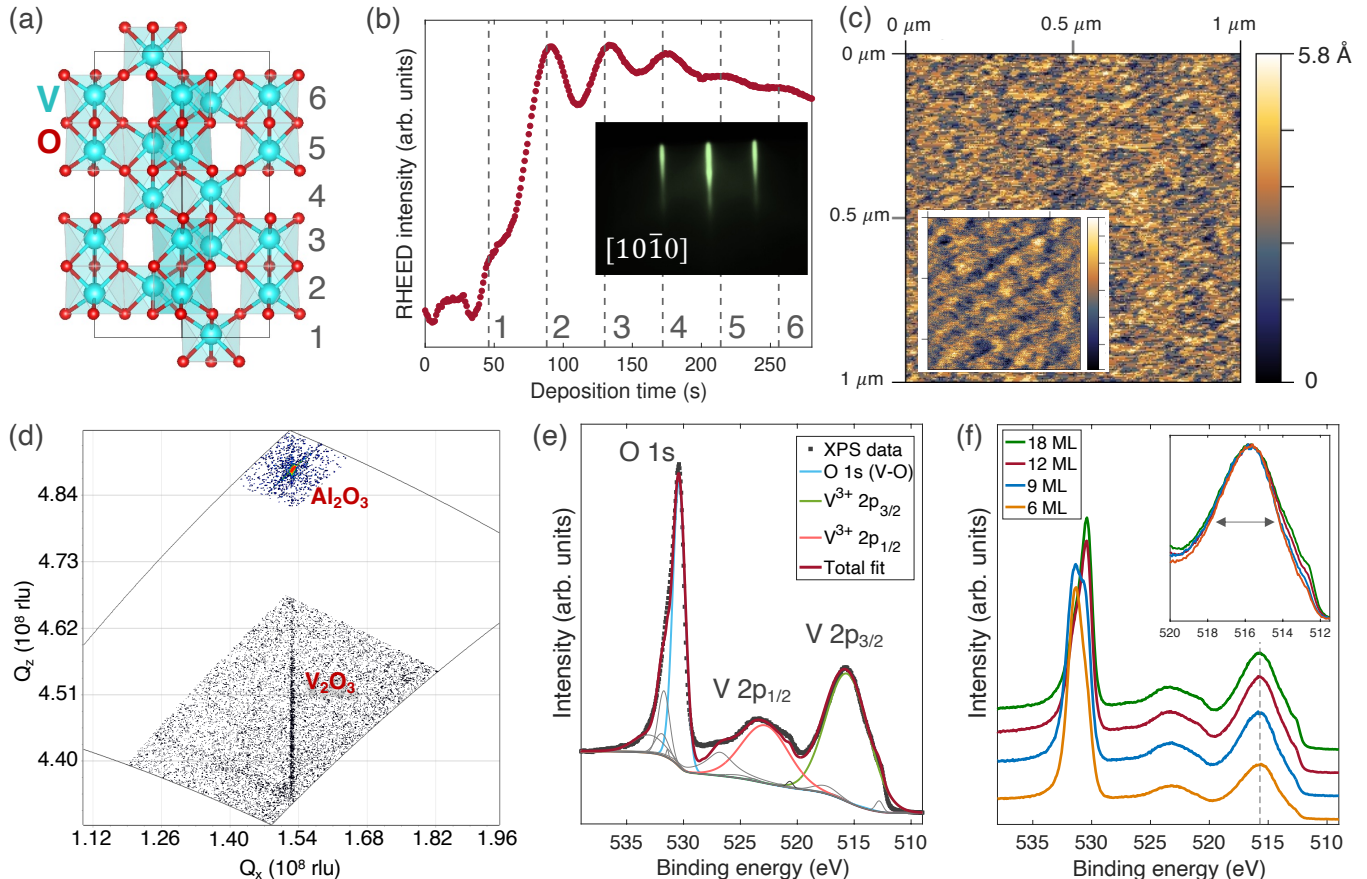


Figure 1. Structural and chemical properties of ultrathin films. (a) The conventional unit cell of V_2O_5 consisting of six monolayers with cyan and red colors corresponding to vanadium and oxygen atoms, respectively. (b) RHEED intensity oscillations as a function of the deposition time where each maximum corresponds to the completion of one atomic layer and with the inset a RHEED pattern taken after the growth. (c) AFM topography of the 18 ML film with the inset an AFM topography of dimension $500 \times 500 \text{ nm}^2$ with a color scale ranging from 0 to 5.6 \AA . (d) RSM of the 18 ML film in the $(10\bar{1}0)$ reflection showing a coherently strained film with identical in-plane lattice constant to the Al_2O_3 substrate. (e) XPS core level O $1s$ - V $2p$ spectrum of the 18 ML with corresponding fitting results for which the V^{3+} components are highlighted while the other stoichiometric components and satellites have been gray colored. The details of the complete fitting result can be found in Fig. S1 of the Supplemental Material. (f) A comparison of the core level O $1s$ - V $2p$ spectra of the different ultrathin films. Note that the O $1s$ level for the 6 and 9 ML thick films consists of both a V-O as well as Al-O component. The inset shows the reducing linewidth of the V $2p_{3/2}$ level upon thickness reduction.

B. Electronics upon thickness reduction

The intrinsic properties of these ultrathin V_2O_5 films at RT were evaluated by the use of transport measurements combined with infrared (IR) spectroscopy. Figure 2 shows the temperature-dependent electrical resistivity $\rho(T)$ of the ultrathin films. First of all, the coherently strained ultrathin films do not show any LT MIT, which has been ascribed to the presence of a large compressive strain and is therefore not related to thickness reduction [18]. The remainder of the manuscript focuses on the room-temperature properties of these ultrathin films.

As a reference, to prove the high-quality of the grown thin films, $\rho(T)$ of a relaxed thin film of 62 nm ($\sim 44 \text{ UC}$) is included in Figure 2a. This shows a sharp discon-

tinuous metal-insulator transition at $\sim 180 \text{ K}$ while the room-temperature resistivity (RTR) equal to $3.94 \cdot 10^{-4} \Omega\text{-cm}$ agrees very well with bulk values [1, 2]. Upon thickness reduction, the RTR value starts to increase, with an abrupt increase below 9 ML. The RTR of 6 ML is nearly five times larger than the $2.3 \Omega\text{-cm}$ RTR value observed in paramagnetic insulating state stabilized for 4% Cr-doped V_2O_5 single crystals [2], and epitaxially strained thin films [5]. Also notice that the 18 ML clearly shows a metallic slope ($d\rho/dT > 0$) at RT, which becomes semi-conducting below with an increasing slope upon confinement indicating an increased electronic bandgap.

To support these transport measurements, the optical reflectance in near-normal angle incidence is measured using FTIR spectroscopy. The optical reflectance, shown

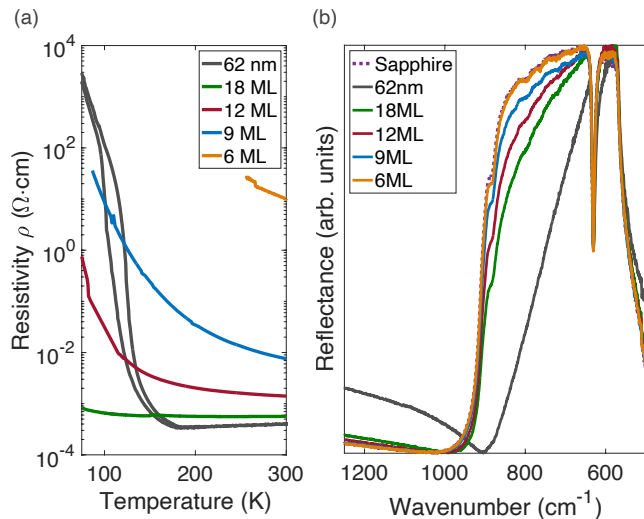


Figure 2. Electronics upon thickness reduction. (a) Temperature-dependent resistivity. (b) Reflectance spectrum near the reststrahlen band of sapphire.

in Figure 2b, has been studied in the mid-infrared range ($480 - 1250 \text{ cm}^{-1}$), close to the reststrahlen band of sapphire, that is the infrared band where the reflectance is near-unity and the IR-active phonon resonances appear. Any metallic thin film leads to a damping of this reststrahlen effect, or thus absorbance by the film. It can be seen that this effect reduces upon reducing thickness. Therefore, it can be concluded that the metallicity disappears below 9 ML thick ultrathin films, in agreement with the transport measurements. A similar spectral change near the reststrahlen band of sapphire can be observed upon LT MIT of the 60 nm thin V_2O_3 film (See Fig. S3 in Supplemental Material).

C. Bandwidth-controlled transition

V_2O_3 is often considered as a key example of a Mott-Hubbard system, that is a purely electronic MIT involving no other degrees of freedom [19–21].

To evaluate the nature of the induced MIT upon thickness reduction, PES was used to probe the changes in the valence band. These spectra consist of a spectral weight derived from the O $2p$ states in the energy range 4 – 10 eV, while close to the Fermi level (E_F), the valence band consists of a broad $V 3d$ weight and a sharp coherent QP weight, as shown in Figure 3a. It should be pointed out that the observation of the coherent QP weight required a high-quality pristine surface, otherwise only a faint shoulder could be identified (see Fig. S2 of the Supplemental Material), which indicates the importance of the surface termination and texture. Moreover, the observation of such a large QP weight in a 18 ML (~ 4.2 nm) film is in excellent agreement with the critical thickness estimate of 4 nm required to see the QP weight, as

determined through angle-resolved PES experiments on single crystal V_2O_3 [22, 23].

Upon thickness reduction, the QP spectral weight starts to vanish at E_F while simultaneously the $V 3d$ band shifts away from E_F opening an energy gap. This also leads to an energy shift of the oxygen (O $2p$) band. The observed vanishing QP weight with a spectral weight transfer to the $V 3d$ band agrees with the bandwidth-controlled Mott transition behavior derived by DMFT, schematically illustrated in Figure 3d [24].

This vanishing QP weight upon confinement can be understood by an orbital-resolved analysis. It was shown that the coherent QP band in the PM phase has a dominant a_{1g} orbital character [23, 25], which transfers its spectral weight to the lower-lying e_g^{π} -derived bands upon transition to the PI state [25–27]. Now, reducing the thickness causes the electron localization in the out-of-plane orbitals, including mainly a_{1g} . In a single-orbital Hubbard model, this corresponds to a reducing effective bandwidth W that triggers a MIT at sufficiently large U/W values with U the on-site Coulomb interactions. This scenario has been observed in many other ultrathin oxide films, often referred to as a dimensional-crossover [28–31].

D. Confinement as an effective stress component

This confinement-induced (dimensional-crossover) MIT has also been observed in various strongly correlated materials [28, 30–32]. However, many of these studies have only considered the electronic nature of this transition, because a structural characterization remains challenging for these few nanometer thick films. In this respect, we have used confocal Raman microscopy and synchrotron X-ray diffraction to study the local interatomic lengths and lattice parameters, respectively.

To monitor local atomic changes in the crystal structure, the Raman active modes have been studied. For V_2O_3 , it is well-known that the A_{1g} Raman mode, illustrated in Figure 4b, can be used to probe the short V-V bond along c axis, as well as the trigonal distortion driving the RT MIT [7, 33, 34]. In particular, a frequency stiffening of the A_{1g} mode observed upon PM to PI MIT is ascribed to an elongated V-V bond where an interelectronic Coulombic force is responsible for the stiffening of the atomic vibration [34, 35]. Taking into account the observed RT MIT in the ultrathin films, the question arises whether the trigonal distortion and the corresponding V-V bond have also been altered upon confinement.

Accordingly, the A_{1g} Raman mode is studied as a function of thickness in the ultrathin films, as shown in Figure 4. To study changes in the phonon dynamics by confinement, the standing wave approximation is proven to be a fruitful approach for many oxides [36–38]. For the trigonal $R\bar{3}c$ symmetry, the Raman active modes are non-

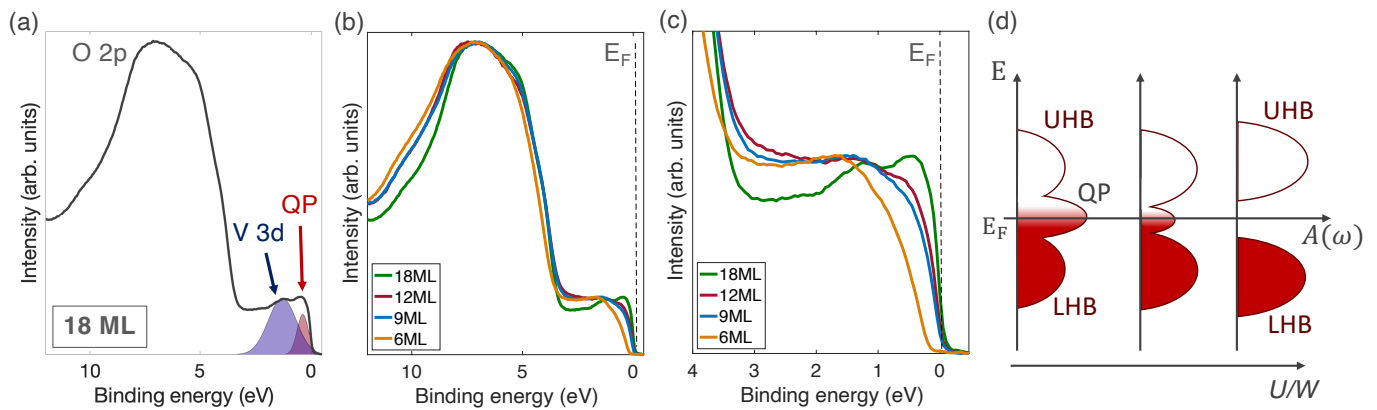


Figure 3. Photoemission spectroscopy. (a) Decomposition of the valence band into $V 3d$ band and QP weight for a film with 18 ML thickness. (b) A comparison of normalized PES spectra of the valence band where (c) the expanded energy scale spectra shows a vanishing QP weight upon thickness reduction. (d) A schematic view of the behavior of the low-energy band structure upon increasing U/W with 3 spectral components: the lower and upper Hubbard bands (LHB/UHB) and the quasiparticle (QP) weight.

polar and can be considered to have a quantized wavevector q along the out-of-plane Brillouin zone branch ($\Gamma-Z$) due to confinement. More specifically, the wavevector q equals $(0, 0, \pi/d)$ with d the number of UCs (6 ML), with the bulk ($d = \infty$) corresponding to the zone-center $\Gamma = (0, 0, 0)$ and the single UC (6ML) to the zone edge $Z = (0, 0, \pi/c)$ with c the out-of-plane lattice constant of the conventional UC. This quantization of the wavevector q also leads to a changing eigenenergy, which can be obtained from the dispersion along the $\Gamma-Z$ branch. The latter was obtained by earlier density functional theory (DFT) calculations [34], and is shown in Fig. 4a.

From the calculated dispersion a softening of the in-plane E_g mode can be inferred upon confinement, while the low-frequency A_{1g} shows an initial softening with an abrupt stiffening close to the zone edge Z . The softening of the E_g mode is confirmed by Raman spectroscopy (see Fig. 4b), albeit that the DFT calculations overestimates the frequency shift. This can be largely explained by the approximation of a sharp boundary condition which prohibits the propagation of the phonon mode across the interface of the film with the substrate. In practice the similarity in crystal structure and phonon spectrum can lead to a broadening of this boundary condition, reducing the effective confinement. On the other hand, a strong frequency hardening is observed for the A_{1g} mode in the Raman spectrum which is inconsistent with the calculated dispersion. This implies that the DFT calculations fail to describe the V-V dimer behavior upon confinement, similar to the PM-PI MIT in bulk V_2O_3 which can only be well-described by DMFT [7]. Moreover, the frequency hardening of the A_{1g} mode upon thickness reduction is very similar to what has been observed in the PM-PI transition, which has been ascribed to a trigonal distortion driving the MIT [34].

At this point, the Raman spectroscopy results ex-

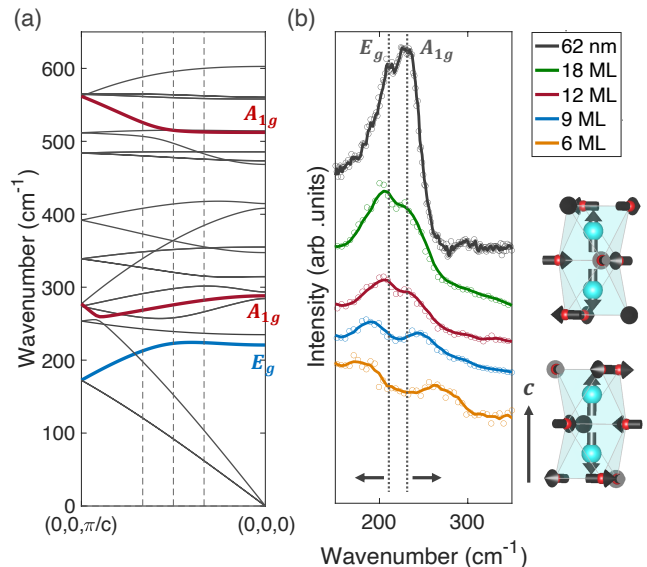


Figure 4. Phonon analysis as a function of thickness. (a) DFT-calculated phonon branch along the (001) direction in the Brillouin zone where $(0, 0, 0)$ corresponds to the zone-center Γ and $(0, 0, \pi/c)$ to the high-symmetry edge point Z . The phonon modes A_{1g} and E_g under investigation are indicated in red and blue, respectively. The dashed lines represent $(0, 0, \pi/d)$ with d corresponding to 18, 12, and 9 ML from right to left. (b) The Raman spectrum in the low-frequency region as a function of thickness with on the right a visualization of the A_{1g} mode where the vectors correspond to the DFT-calculated eigenvectors of the low-frequency vibration. For visual purposes the eigenvectors have been scaled.

clude any change in symmetry, that means, the RT MIT is *isosymmetric*. However, this does not exclude an isostructural MIT as often misinterpreted. To verify whether there is a structural change, synchrotron X-ray

diffraction was performed on 9 ML and 18 ML ultrathin films to determine the out-of-plane c lattice constant. A decrease of the c lattice parameter is observed upon thickness reduction from 18 ML to 9 ML, i.e. there is a change in c/a ratio, quantifying the trigonal distortion (See Fig. S5 in Supplemental Material). The relative change of the c/a between 18 ML and 9 ML equals 2.59 %, which is larger than the relative change of 1.32 % for the bulk PM-PI transition. These results confirm the structural nature of this confinement-induced MIT, where a trigonal distortion is triggered upon thickness reduction. This out-of-plane strain component suggests that dimensional confinement acts as an alternative stress term to alter the trigonal distortion triggering the MIT in V_2O_3 .

IV. DISCUSSION

Although size confinement has been considered as a chemical pressure in many nanostructures [39], such as nanowires [40], it remains unnoticed how confinement in thin films and superlattices can lead to an effective out-of-plane pressure. Therefore, we aim to provide an intuitive picture to perceive dimensional confinement as an effective (chemical) pressure. Firstly, by defining pressure in the material as $dP = -KdV/V$ with K the bulk modulus, it is evident that an induced pressure exists when there is a change in volume V . In particular, considering $K > 0$, a positive pressure P corresponds to $dV < 0$, while $dV > 0$ is associated with a negative induced pressure. Reversely, changing the volume in a controlled manner can lead to the inducement of a positive or negative pressure/stress. Now, (chemical) pressure and chemical bonds are intimately related, to the extent that (chemical) pressure has been used as an effective way to identify and quantify the chemical bonds driving the displacive phase transitions [41, 42]. Therefore, we propose two views on how a change in pressure (dP) or volume (dV) alters the electrons and their hybridization state. (1) A positive pressure tends to narrow the electron density distribution leading to an orbital expansion to decrease the energy, while negative pressure is accompanied with interatomic delocalization in the regions where covalent bonding occurs [43]. (2) Alternatively, by approximating the kinetic (KE) and potential (PE) energies of electrons by the volume dependences $V^{-2/3}$ and $V^{-1/3}$ respectively, it becomes immediately evident that a change of volume, or thus a pressure term, can be directly linked to a change in the hybridization (PE/KE) of the electrons [44].

In this way, pressure can be perceived as an effective way to alter the electronic charge distribution and their corresponding bonds. Reversely, altering the electronic charge distribution leads to a (chemical) pressure within the crystal. Therefore, dimensional confinement reducing the KE of the electrons occupying the out-of-plane orbitals leads to an increased hybridization (PE/KE $\sim V^{1/3}$), and thus also results in an effective

negative pressure term.

Accordingly, the structural changes (out-of-plane strain) discussed in Section IIID can be explained by an out-of-plane stress that is strongly coupled to the enhanced hybridization of the a_{1g} orbital, which triggers the MIT. Similarly, many other physical phenomena in ultrathin films and heterostructures can be explained as for example, the enhanced tetragonality in various perovskites, such as $PbTiO_3$, $BaTiO_3$, and $SrTiO_3$ [45]. This involves the electron localization in the out-of-plane π -bonding orbitals which favors the hybridization with the O $2p$ orbitals strengthening the tetragonal distortion [46, 47]. Similarly, it can be expected that the suppression/enhancements of octahedral rotations in perovskite-based heterostructures can be explained by the same hybridization preference upon confinement [48].

Consequently, by combining epitaxial substrate-induced strain with thickness control of the ultrathin films, a three-dimensional strain can be imposed albeit that the out-of-plane component is uni-directional whose sign depends on the electronic configuration.

V. CONCLUSIONS

The achievement of the atomic layered growth of this archetypical Mott material V_2O_3 has enabled the observation of an intrinsic MIT at RT induced by dimensional confinement. It has been identified as a clear illustration of a bandwidth-controlled Mott-Hubbard transition with a vanishing QP below 18 ML. Moreover, our findings highlight an enhanced trigonal distortion under confinement, emphasizing the structural component of this MIT. The observed distortion suggests the possibility to model confinement along a specific direction as a negative stress component. Thereby illustrating the potential to leverage thickness control in ultrathin films or heterostructures to induce an effective out-of-plane stress.

ACKNOWLEDGEMENTS

Part of this work was financially supported by the KU Leuven Research Funds, Project No. C14/21/083, iBOF/21/084, No. KAC24/18/056 and No. C14/17/080, as well as the FWO AKUL/13/19 and AKUL/19/023, and the Research Funds of the INTERREG-E-TTEST Project (EMR113) and INTERREG-VL-NL-ETPATHFINDER Project (0559). Part of the computational resources and services used in this work were provided by the VSC (Flemish Supercomputer Center) funded by the Research Foundation Flanders (FWO) and the Flemish government. We acknowledge the use of synchrotron radiation facility at BM25-SpLine at the European Synchrotron and we thank the Consejo Superior de Investigaciones Científicas and the Ministerio de Ciencia e Innovación for financial support under the

proposal MA-5601 and projects PIE 2010 6 0E 013 and PIE 2021 60 E 030. J. S. L. acknowledges financial support from the Ministerio de Asuntos Económicos y Transformación Digital (MINECO) through the project PID2020-114192RB-C41. M. M. acknowledges support from Severo Ochoa Programme for Centres of Excellence in R&D (MINCINN, Grant CEX2020-001039-S).

AUTHOR CONTRIBUTIONS

S.M., J.P., J.W.S. and M.H. conceived the conceptual idea and devised the research plan. S.M. executed the

synthesis, while in-house diffraction, transport and optical experiments were carried out by S.M., C.B. and W.F.H. XPS, AFM and ARUPS were performed by K.S. Raman spectroscopy was conducted by J.S.L. Synchrotron X-ray diffraction was executed by S.M., W.F.H. and M.M. under guidance of J.S.L. and J.R.Z. All analysis and preparation of the manuscript were done by S.M. All co-authors reviewed and revised the manuscript.

COMPETING INTERESTS

The authors declare no competing interests.

-
- [1] D. B. McWhan, T. M. Rice, and J. P. Remeika, *Phys. Rev. Lett.* **23**, 1384 (1969).
- [2] D. B. McWhan and J. P. Remeika, *Phys. Rev. B* **2**, 3734 (1970).
- [3] F. Rodolakis, P. Hansmann, J.-P. Rueff, A. Toschi, M. W. Haverkort, G. Sangiovanni, A. Tanaka, T. Saha-Dasgupta, O. K. Andersen, K. Held, M. Sikora, I. Aliot, J.-P. Itié, F. Baudalet, P. Wzietek, P. Metcalf, and M. Marsi, *Phys. Rev. Lett.* **104**, 047401 (2010).
- [4] P. Homm, L. Dillemans, M. Menghini, B. Van Bilzen, P. Bakalov, C.-Y. Su, R. Lieten, M. Houssa, D. Nasr Esfahani, L. Covaci, F. M. Peeters, J. W. Seo, and J.-P. Locquet, *Applied Physics Letters* **107**, 111904 (2015).
- [5] P. Homm, M. Menghini, J. W. Seo, S. Peters, and J. P. Locquet, *APL Materials* **9**, 021116 (2021).
- [6] D. Grieger and F. Lechermann, *Phys. Rev. B* **90**, 115115 (2014).
- [7] A. I. Poteryaev, J. M. Tomczak, S. Biermann, A. Georges, A. I. Lichtenstein, A. N. Rubtsov, T. Saha-Dasgupta, and O. K. Andersen, *Phys. Rev. B* **76**, 085127 (2007).
- [8] M. Pickem, J. Kaufmann, K. Held, and J. M. Tomczak, *Phys. Rev. B* **104**, 024307 (2021).
- [9] B. Klebel-Knobloch, T. Schäfer, A. Toschi, and J. M. Tomczak, *Phys. Rev. B* **103**, 045121 (2021).
- [10] S. Mellaerts, R. Meng, M. Menghini, V. Afanasiev, J. W. Seo, M. Houssa, and J.-P. Locquet, *npj 2D Materials and Applications* **5**, 65 (2021).
- [11] C. Ponchut, J. M. Rigal, J. Clément, E. Papillon, A. Homs, and S. Petitdemange, *Journal of Instrumentation* **6**, C01069 (2011).
- [12] H. A. Wriedt, *Bulletin of Alloy Phase Diagrams* **10**, 271 (1989).
- [13] N. Bahlawane and D. Lenoble, *Chemical Vapor Deposition* **20**, 299 (2014).
- [14] G. Silversmit, D. Depla, H. Poelman, G. B. Marin, and R. De Gryse, *Journal of Electron Spectroscopy and Related Phenomena* **135**, 167 (2004).
- [15] G. A. Sawatzky and D. Post, *Phys. Rev. B* **20**, 1546 (1979).
- [16] Q. Luo, Q. Guo, and E. G. Wang, *Applied Physics Letters* **84**, 2337 (2004).
- [17] V. Polewczyk, S. Chaluvadi, D. Dagur, F. Mazzola, S. Punathum Chalil, A. Petrov, J. Fujii, G. Panaccione, G. Rossi, P. Orgiani, G. Vinai, and P. Torelli, *Applied Surface Science* **610**, 155462 (2023).
- [18] L. Dillemans, T. Smets, R. R. Lieten, M. Menghini, C.-Y. Su, and J.-P. Locquet, *Applied Physics Letters* **104** (2014), 10.1063/1.4866004.
- [19] M. Imada, A. Fujimori, and Y. Tokura, *Rev. Mod. Phys.* **70**, 1039 (1998).
- [20] K. Held, G. Keller, V. Eyert, D. Vollhardt, and V. I. Anisimov, *Phys. Rev. Lett.* **86**, 5345 (2001).
- [21] P. Hansmann, A. Toschi, G. Sangiovanni, T. Saha-Dasgupta, S. Lupi, M. Marsi, and K. Held, *physica status solidi (b)* **250**, 1251 (2013).
- [22] G. Borghi, M. Fabrizio, and E. Tosatti, *Phys. Rev. Lett.* **102**, 066806 (2009).
- [23] F. Rodolakis, B. Mansart, E. Papalazarou, S. Gorovikov, P. Vilmercati, L. Petaccia, A. Goldoni, J. P. Rueff, S. Lupi, P. Metcalf, and M. Marsi, *Phys. Rev. Lett.* **102**, 066805 (2009).
- [24] A. Georges, G. Kotliar, W. Krauth, and M. J. Rozenberg, *Rev. Mod. Phys.* **68**, 13 (1996).
- [25] M. Thees, M.-H. Lee, R. L. Bouwmeester, P. H. Rezende-Gonçalves, E. David, A. Zimmers, F. Fortuna, E. Frantzeskakis, N. M. Vargas, Y. Kalcheim, P. L. Fèvre, K. Horiba, H. Kumigashira, S. Biermann, J. Trastoy, M. J. Rozenberg, I. K. Schuller, and A. F. Santander-Syro, *Science Advances* **7**, eabj1164 (2021).
- [26] J.-H. Park, L. H. Tjeng, A. Tanaka, J. W. Allen, C. T. Chen, P. Metcalf, J. M. Honig, F. M. F. de Groot, and G. A. Sawatzky, *Phys. Rev. B* **61**, 11506 (2000).
- [27] I. Lo Vecchio, L. Baldassarre, F. D'Apuzzo, O. Limaj, D. Nicoletti, A. Perucchi, L. Fan, P. Metcalf, M. Marsi, and S. Lupi, *Phys. Rev. B* **91**, 155133 (2015).
- [28] K. Yoshimatsu, T. Okabe, H. Kumigashira, S. Okamoto, S. Aizaki, A. Fujimori, and M. Oshima, *Phys. Rev. Lett.* **104**, 147601 (2010).
- [29] M. Gu, J. Laverock, B. Chen, K. E. Smith, S. A. Wolf, and J. Lu, *Journal of Applied Physics* **113**, 133704 (2013).
- [30] E. Sakai, M. Tamamitsu, K. Yoshimatsu, S. Okamoto, K. Horiba, M. Oshima, and H. Kumigashira, *Phys. Rev. B* **87**, 075132 (2013).
- [31] M. Gu, S. A. Wolf, and J. Lu, *Advanced Materials Interfaces* **1**, 1300126 (2014).
- [32] D. Shiga, B. E. Yang, N. Hasegawa, T. Kanda, R. Tokunaga, K. Yoshimatsu, R. Yukawa, M. Kitamura, K. Horiba, and H. Kumigashira, *Phys. Rev. B* **102**,

- 115114 (2020).
- [33] N. Kuroda and H. Y. Fan, *Phys. Rev. B* **16**, 5003 (1977).
- [34] W.-F. Hsu, S. Mellaerts, C. Bellani, P. Homm, N. Uchida, M. Menghini, M. Houssa, J. W. Seo, and J.-P. Locquet, *Phys. Rev. Mater.* **7**, 074606 (2023).
- [35] H. Yang and R. J. Sladek, *Phys. Rev. B* **32**, 6634 (1985).
- [36] P. Senet, P. Lambin, and A. A. Lucas, *Phys. Rev. Lett.* **74**, 570 (1995).
- [37] J. Prempfer, F. O. Schumann, A. Dhaka, S. Polzin, K. L. Kostov, V. Goian, D. Sander, and W. Widdra, *physica status solidi (b)* **257**, 1900650 (2020).
- [38] A. Schober, J. Fowlie, M. Guennou, M. C. Weber, H. Zhao, J. Iniguez, M. Gibert, J.-M. Triscone, and J. Kreisel, *APL Materials* **8**, 061102 (2020).
- [39] K. Lin, Q. Li, R. Yu, J. Chen, J. P. Attfield, and X. Xing, *Chem. Soc. Rev.* **51**, 5351 (2022).
- [40] J. Sun, Q. Li, H. Zhu, Z. Liu, K. Lin, N. Wang, Q. Zhang, L. Gu, J. Deng, J. Chen, and X. Xing, *Advanced Materials* **32**, 2002968 (2020).
- [41] J. Engelkemier and D. C. Fredrickson, *Chemistry of Materials* **28**, 3171 (2016).
- [42] H. H. Osman, M. A. Salvadó, P. Pertierra, J. Engelkemier, D. C. Fredrickson, and J. M. Recio, *Journal of Chemical Theory and Computation* **14**, 104 (2018).
- [43] H. H. Osman, M. A. Salvadó, P. Pertierra, J. Engelkemier, D. C. Fredrickson, and J. M. Recio, *Journal of Chemical Theory and Computation* **14**, 104 (2018).
- [44] S. Mellaerts, J. W. Seo, V. Afanas'ev, M. Houssa, and J.-P. Locquet, *Phys. Rev. Mater.* **6**, 064410 (2022).
- [45] C.-C. Chiu, S.-Z. Ho, J.-M. Lee, Y.-C. Shao, Y. Shen, Y.-C. Liu, Y.-W. Chang, Y.-Z. Zheng, R. Huang, C.-F. Chang, C.-Y. Kuo, C.-G. Duan, S.-W. Huang, J.-C. Yang, and Y.-D. Chuang, *Nano Letters* **22**, 1580 (2022).
- [46] H. Thomann, *Ferroelectrics* **73**, 183 (1987).
- [47] R. E. Cohen, *Nature* **358**, 136 (1992).
- [48] P. Garcia-Fernandez, J. A. Aramburu, M. T. Barriuso, and M. Moreno, *The Journal of Physical Chemistry Letters* **1**, 647 (2010).